Pharm Res (2012) 29:460–470
DOI 10.1007/s11095-011-0574-7

RESEARCH PAPER

Polymorph Formation and Nucleation Mechanism of Tolfenamic Acid in Solution: An Investigation of Pre-nucleation Solute Association

Alessandra Mattei • Tonglei Li

Received: 27 April 2011 / Accepted: 15 August 2011 / Published online: 31 August 2011

ABSTRACT

Purpose Crystallization from solution involves nucleation and growth; growth conditions greatly influence self-association behaviors of solute molecules in these steps, affecting crystal packing of organic molecules. We examined the role of pre-nucleation association to provide insights into the mutual influence between molecular conformation in solution and packing in the solid state.

Methods Crystallization experiments of tolfenamic acid were conducted in ethanol under different supersaturation conditions. UV spectroscopy was performed to study self-association of solute molecules in ethanol as a function of concentration. Intermolecular interaction energies of tolfenamic acid dimers were calculated with quantum mechanical methods.

Results As supersaturation increased, growth of the most stable polymorph outpaced the metastable one, contradicting Ostwald's Rule of Stages. UV spectroscopy measurement suggests solute molecules exist as hydrogen-bonded dimers and more dimers form as total concentration increases. Hydrogen bonding in the most stable form is significantly stronger than that in the metastable form.

Conclusions With the fact that molecular conformation is different in the two polymorphs, as concentration increases, solute molecules rearrange their conformations to form stronger hydrogen-bonded dimers in solution, resulting in nucleation of the most stable form.

KEY WORDS dimer · nucleation · polymorph · self-association · supersaturation

A. Mattei • T. Li (✉)
Department of Pharmaceutical Sciences
University of Kentucky
Lexington, Kentucky, USA
e-mail: tonglei@uky.edu

INTRODUCTION

Polymorphism of drug compounds plays a key role in formulation and manufacturing design; screening of polymorphic structures is thereby one of the major undertakings in pharmaceutical industry (1,2). On account of this, prediction and precise control of a specific polymorph are critical for achieving desired solubility and stability requirement. Recent efforts have been devoted to the development of consistent and reliable crystallization processes for producing desirable polymorphs, including on-line, spectroscopy-based monitoring designs of crystal growth in solution (3–5). Polymorphic formation is known to be affected by a wide variety of growth conditions, such as type of solvent (6–8), supersaturation (4,9), temperature (10), and use of additives (11,12). Despite considerable efforts studying crystallization mechanism, understanding of kinetic factors that govern polymorphic formation in solution largely remains limited (13).

Crystallization from solution generally involves nucleation and growth. Nucleation starts from formation of small embryos of a new crystalline phase in a supersaturated solution. Because of the creation of the solid surface, a free energy penalty is generally associated with the appearance of the nuclei. Overcoming the nucleation energy barrier dynamically depends on supersaturation as well as molecular packing of nuclei. Early events of nucleation thus play a decisive role in determining the resultant crystal structure (14,15). An active viewpoint is that solute molecules may form supramolecular, pre-nucleation species, which act as the precursors of crystal growth (16). The underlying connection between the existence of pre-nucleation solute entities and final crystal structures, which is focused by this report, further illustrates the intricacy and importance of molecular interaction throughout the embryonic process. Needless to say, nucle-

ation has been recognized and described by various models, but it is far from being clearly understood (17).

Classical nucleation theory (CNT) has been widely used in explaining nucleation kinetics (18–20). The thermodynamic approach characterizes crystal growth by macroscopic quantities of surface and bulk free energies, taking no account of molecular features of a growing system. It assumes that the molecular structure of a nucleus is the same as that of the final crystal. However, recent studies suggest that pre-nucleation aggregates or clusters exist in solution and may be structurally different from individually solvated solute molecules (15,21,22). Moreover, CNT regards formation of a metastable polymorph as bearing a smaller surface energy and subsequently overgrowing the most stable form (i.e., Ostwald's Rule of Stages) (23). Yet, there are cases of crystallization where the most stable forms always appear the first (11,24).

Recognition of the existence of pre-nucleation aggregates as well as recent crystallization kinetic studies have set the stage to move beyond CNT (25,26). Computational simulations (27,28) and experimental studies of proteins (25,29,30) imply the possibility that nucleation comprises at least two stages, aggregation of solute molecules into a disorderly packed ensemble and subsequent reorganization of such a cluster from which crystals nucleate. Formation of a transient phase prior to transforming to the packing structure adopted by the bulk is shown to be a common feature observed not only by macromolecular systems (31), but also by relatively small molecules (32,33). A free energy advantage may be gained by forming a transient cluster and subsequent crystallizing, instead of following the classical route directly from individual solute molecules to the formation of structured crystalline nuclei (25,26). Correspondingly, the nucleation rate is only determined by the assembling kinetics of transient clusters (34). Such theorem contradicts the paradigm of CNT (17,26).

Additional studies also speculate that pre-nucleation aggregates may not necessarily be randomly packed; rather, they may bear the resemblance of the structure adopted by the subsequently crystallized solid phase. This has been reported in the growth of 2,6-dihydroxybenzoic acid (35). It was found that carboxylic acid dimers were present predominately in toluene from which a dimer-based crystal form was produced, while polymeric aggregates appeared to dominate in chloroform, leading to a hydrogen-bonded catemer observed in the harvested crystal structure. Similar behaviors were observed for tetrolic acid (36). In chloroform, hydrogen-bonded dimers were present giving rise to a dimeric polymorph; dimers were nonetheless absent in ethanol, from which a catemer-based crystal was obtained. Solution chemistry of glycine has been also extensively studied (21,37,38). Based on observations by atomic force microscopy and grazing incidence X-Ray diffraction (15,39), it is suggested that glycine molecules in neutral aqueous solutions behave primarily as hydrogen-bonded dimers resulting in a crystal structure where the dimer motif is retained. Note that the speculation, mainly based on the measurement of the nucleation process at the crystal-liquid interface, is recently questioned (40).

These efforts illustrate the complicated nature of nucleation, and understanding of molecular mechanism during nucleation largely remains speculative and scarce. In our studies of crystal growth, there are several key questions to be addressed, including (1) what role the solute association plays on polymorphic formation, (2) whether molecular conformation influences the solute association, and (3) how intermolecular interactions in the solute aggregates determine the molecular packing in the final crystal structure. In this particular study, the critical role of pre-nucleation association is examined by combining experimental study and quantum mechanical calculation. The focus lies in the recognition of intermolecular interactions that determine molecular conformation and packing in solution and crystal. For this purpose, tolfenamic acid (TFA, Fig. 1), a nonsteroidal anti-inflammatory drug (NSAID), is selected as the model system. Five structurally characterized polymorphs of TFA have been reported in the literature, displaying conformational polymorphism (41,42). The two mostly encountered structures, forms I (colorless form) and II (yellow form), are studied in this work. The conformation of the molecules in form I and form II differs mainly in the torsion angle τ_1 (−74.9° and −142.6° of forms I and II, respectively). Similar hydrogen-bonded dimer motifs between neighboring carboxyl groups exist in the two forms (Fig. 2). The conformational polymorphism and intermolecular hydrogen-bonding make TFA a proper case for studying the pre-nucleation behavior and examining the influence of intermolecular interactions on the crystallization outcome.

MATERIALS AND METHODS

Materials

Tolfenamic acid (MW = 261.70, >97% purity) was purchased from TCI America (Portland, OR) and was recrystallized from ethanol to obtain pure form I. TFA

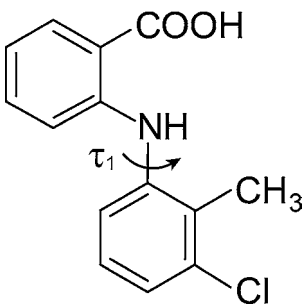

Fig. 1 Molecular structure of TFA, defining the torsion angle τ_1 differing among the conformers.

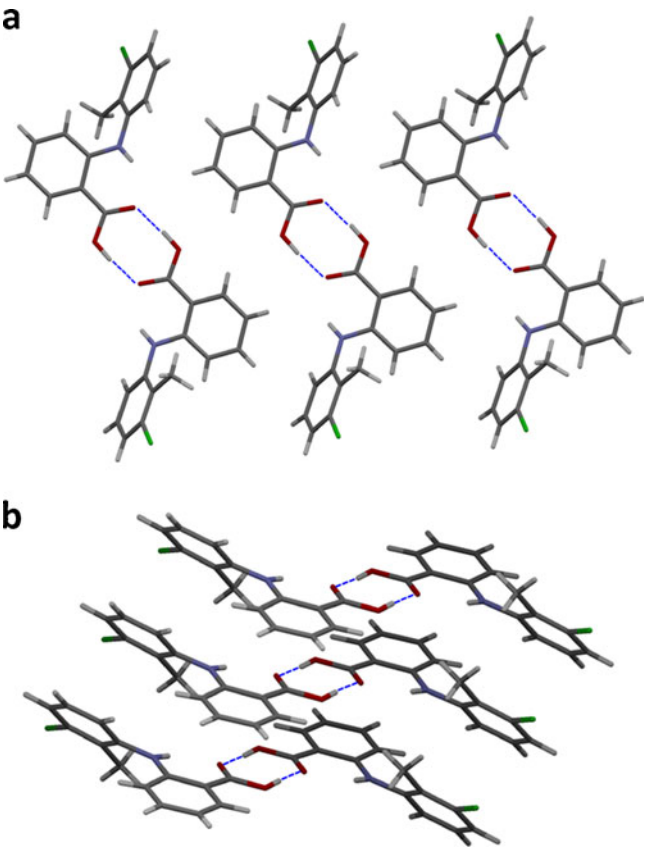

Fig. 2 Hydrogen-bonded dimer motifs of TFA form I (**a**) and form II (**b**) (41). Hydrogen-bonding is denoted as dash line.

form II was crystallized by rapid cooling of an ethanol solution to 25°C. The purity was verified (see below). Ethanol (>99.9% purity) was obtained from Decon Labs, Inc. (King of Prussia, PA) and was used as received.

Powder X-Ray Diffraction (PXRD)

The polymorphic purity and identification were assessed using a powder X-ray diffractometer (Multiflex, Rigaku Co., The Woodlands, TX) with Cu Kα radiation operating at 40 kV and 44 mA. Samples were scanned over a 2θ range of 5–40° at the rate of 2°/min. Reference powder patterns of TFA crystals were calculated with Mercury 1.4 (The Cambridge Crystallographic Data Centre, Cambridge, UK) based on respective single crystal structures (41) for comparison with experimental data.

Differential Scanning Calorimetry (DSC)

Thermograms of TFA forms I and II were recorded using a Q20 DSC (TA Instruments, New Castle, DE). The temperature scale and heat flow were calibrated by measuring the onset temperature and the enthalpic response of an Indium standard. Samples (3–5 mg) were respectively placed in hermetically sealed aluminum pans and heated from 40°C to 240°C at a heating rate of 20°C/min under a helium purge. Data were analyzed with TA Universal Analysis software v. 4.5A.

Attenuated Total Reflectance Fourier Transform Infrared (ATR-FTIR) Spectroscopy

A Varian FTS-7000e FTIR spectrometer (Varian Inc., Palo Alto, CA) equipped with a DTGS detector and a PIKE MIRacle ATR ZnSe accessory was employed for all the experiments. Each spectrum represented 32 co-added scans measured at a spectral resolution of 8 cm^{-1} over the wavenumber range of 4,000–600 cm^{-1}. A background spectrum (without the sample) was collected under the same experimental conditions and was subtracted from each sample spectrum. Spectral data were acquired with Varian Resolutions Pro software.

Known ratios of TFA pure polymorphs were prepared by gently mixing a total weight of 100 mg to obtain a set of standards for the construction of a standard curve for quantitative polymorph analysis. Each calibration sample was analyzed in triplicate.

Solubility Determinations

The solubilities of forms I and II of TFA were measured in ethanol at 37°C. An amount of the pure solid polymorphs well in excess of their solubility was allowed to equilibrate with approximately 3 mL of solvent in a 7-mL borosilicate vial. The sealed vial was rotated in an incubator (VWR Scientific Inc., San Francisco, CA) set at the desired temperature for at least 72 h. An aliquot of the saturated solution was then taken at various time intervals, filtered through a Millipore filter (0.45 μm pore size), and diluted to an appropriate concentration for spectrophotometric UV analysis at 286 nm (Shimadzu 1800, Columbia, MD). The maximum concentration of the dissolved metastable form, before declining toward the corresponding plateau value of the stable form, was assumed as its apparent solubility. Equilibration was reached when the concentration of three consecutive measurements differed less than 2%. Residual solid phase after equilibration in ethanol solution for 72 h was identified by PXRD analysis. The solubility of each sample was measured in triplicate. Solubility data were used to define the initial supersaturation (i.e., ratio between concentration and solubility) with respect to form I in ethanol.

Grinding and Slurry Crystallization Experiments

Solvent-drop grinding of pure forms I and II was carried out using ethanol. In separate experiments, pure forms I and II were taken in a mortar and pestle and subjected to

grinding while a few droplets of ethanol were added intermittently. Similarly, a 1:1 polymorphic mixture of the two forms was subjected to ethanol-assisted grinding. The ground samples were analyzed by PXRD.

Slurry-crystallization experiment was performed by slowly stirring a slurry of TFA form II (30 mg) in a 7-mL borosilicate vial with 1 mL of ethanol at room temperature. The resultant sample was analyzed by PXRD.

Crystallization Experiments

Experiments were carried out using 100 mL three neck flask with an impeller stirring at 100 rpm. Solutions were prepared by dissolving the required amounts of TFA form I in ethanol at about 60°C. Following complete dissolution, the solutions at various concentrations (supersaturation) were filtered through a warmed 0.2 μm syringe filter, transferred to the three neck flask, and then cooled rapidly to 37°C by a temperature-controlled water bath. Liquid-phase samples were removed through a 0.45 μm syringe filter at known time intervals, diluted, and analyzed by UV spectroscopy for the solute concentration measurement. Samples of the solid phase were also taken at predetermined time intervals, air dried, and subjected to ATR-FTIR spectroscopy for polymorphic composition analysis. The solid isolated from the suspension was also analyzed with PXRD to identify the form of the solid.

To test the validity of the crystallization method, experiments were also conducted by dissolving TFA form II in ethanol in order to verify whether the structure of the starting, dissolved material would affect crystallization kinetics. Moreover, to ensure that no (detectable) nucleation occurred during the filtration step and that all particles were dissolved, solutions were maintained at the heating temperature for 2 h and subsequently cooled without filtration. It was observed that neither the initial polymorph of the drug nor the filtration played a noticeable role in the crystallization process.

Seeding experiments were performed by adding 1 wt % (based on the total mass of TFA) of dried, ground seed crystals of either form I or II to ethanol solutions at different supersaturation ratios. Following seeding, the solutions were crash cooled to 37°C and changes in solution concentration as well as in solid composition were monitored over time, as previously described for the unseeded experiments.

Self-Association Measurements

The study of self-association was carried out by measurements of UV spectroscopy over the concentration range 5.76×10^{-5}–2.30×10^{-2} M in ethanol at room temperature. The method is based on the detection of deviation from the Beer-Lambert law with increasing concentration (43,44). Appropriate amounts of the drug were added to volumetric flasks and diluted with absolute ethanol. Each sample was prepared in triplicate. Absorbance spectra of the resultant solutions were recorded in a spectrophotometer (Shimadzu 1800) with quartz cells of path length 10, 1, or 0.1 mm at 346 nm when appropriate. The band at 346 nm corresponds to the n-π* electronic transition of TFA that is suitable to study the mode of molecular assembly (44). The path length of a cuvette was calibrated using potassium chromate solution (45). From the absorbance of solutions, apparent molar absorptivities were calculated as a function of solute concentration. A mathematical model was applied to fit the apparent molar absorptivity *versus* concentration profiles. The curve fitting was performed by non-linear least squares regression analysis (Scientist, Micromath Scientific Software, St. Louis, MO).

Computational Methods

The major difference in the molecular conformation of forms I and II stems from the torsion angle τ_1 (Fig. 1). In order to calculate the difference in hydrogen-bonding strength between the two forms, the two dimer configurations were taken directly from the respective crystal structures of TFA polymorphs (41). Each dimer then underwent constrained optimization with τ_1 and the intermolecular distances between oxygen atoms of the hydrogen-bonded carboxyl groups held constant while all bond distances, bond angles, and other torsion angles were allowed to be optimized. The optimization was carried out at the level of B3LYP/6-31G(d,p) using the Gaussian 03 package (46). Root-mean-square (RMS) values of Cartesian coordinates of TFA dimers due to the optimization were insignificant, 0.021 and 0.009 Å of form I and II dimers, respectively, indicating that the optimization preserved the dimer configurations, particularly the τ_1 angle, from the crystal structures. Intermolecular interaction energies of the optimized cyclic dimers were then calculated in gas phase at two different levels of B3LYP/6-31+G(d,p) and MP2/6-31+G(d,p). The basis set with diffuse orbitals was selected to improve the description of hydrogen-bonding (47). The basis set superposition error was corrected by the counterpoise method when calculating the intermolecular energies (48).

Lattice energies of the two TFA polymorphs were calculated with an empirically augmented density functional theory (DFT) method (49,50). It is well known that a typical DFT cannot fully consider van der Waals interactions (51–53), as in the program we used. To circumvent the limitation, the crystal structures were firstly optimized with the lattice parameters held constant while allowing fractional coordinates of all atoms to adjust. This approach proved fairly acceptable because of the long-range, weak,

and un-directional nature of van der Waals forces that have little impact on fractional coordinates when the lattice parameters are kept fixed during optimization (49,50). The basis set used was B3LYP/6-21G(d,p); no diffuse orbitals were included due to potential instability introduced to Bloch functions. RMS values of optimized Cartesian coordinates were 0.011 and 0.026Å for forms I and II, respectively, demonstrating that the optimization corrected minor structural uncertainties likely induced by hydrogen positions that were assigned—a common practice in X-ray structure determination. The single-point energy of optimized crystal structures was then calculated and, according to the optimized atomic coordinates, the van der Waals energy component was included *post priori*. The van der Waals energy was evaluated by a damped analytical model that was based on interatomic distances and empirical parameters (54,55). The lattice energy was derived as the difference between the total corrected energy of a crystal system and the lowest energy of a fully optimized single molecule in vacuum. In addition, we calculated the difference between the total corrected energy of a crystal system and the gas-phase energy of a single molecule having the same conformation as in the crystal; we called it crystallization energy. A periodical quantum mechanical program, CRYSTAL06 (56), was used for the optimization and energy calculations of TFA crystal structures. Energy convergence for the calculations was set at 10^{-7} Hartree. Root-mean-squares of the energy gradient and atomic displacement were set at 0.0001 and 0.0003 atomic units, respectively.

RESULTS AND DISCUSSION

Characterization of Tolfenamic Acid Polymorphs

Tolfenamic acid samples prepared in our laboratory show similar morphology of both forms I and II (Fig. 3). Solubility profiles of TFA forms I and II were measured in ethanol (Fig. 4). The solution concentration, when form II was used as the starting material, increased until it reached a maximum around the solubility of the metastable polymorph, which should be regarded as an "apparent" value because thermodynamic equilibrium could not be reached when measuring the metastable form. Then, the concentration declined toward the corresponding plateau value of the stable form I and remained at that concentration thereafter for 72 h, showing a typical solvent-mediated phase transition (1,57). The residual solid samples were verified to be form I regardless of the starting materials. The thermodynamic solubility in ethanol is then estimated to be 8.61×10^{-2} M (22.54 mg/mL) at 37°C, while the apparent value of form II is 9.56×10^{-2} M (25.01 mg/mL).

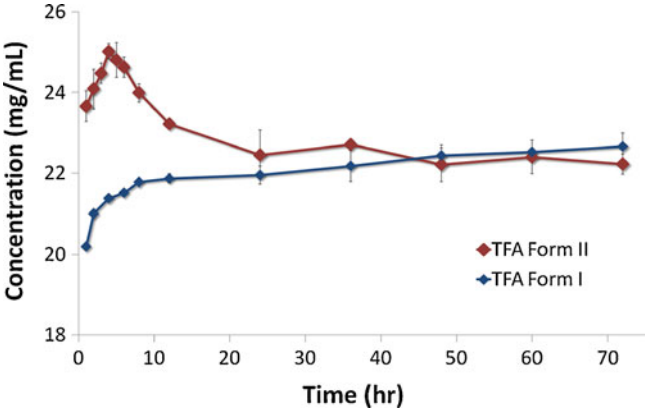

Fig. 4 Solubility profiles of forms I and II of TFA in ethanol at 37°C, determined using UV spectroscopy ($n = 3$).

The relative stability of forms I and II was inferred by the solvent-mediated phase transition as well as experiments of solvent-drop grinding, slurry crystallization, and thermal analysis. When form II was subjected to ethanol-assisted grinding in a mortar and pestle, conversion to form I occurred after 1 h, as monitored by PXRD (Fig. 5). No phase conversion was observed for the pure form I. When a polymorphic mixture of the two forms was subjected to ethanol-assisted grinding, phase transformation occurred readily to give form I within 20 min. In addition, slurry of

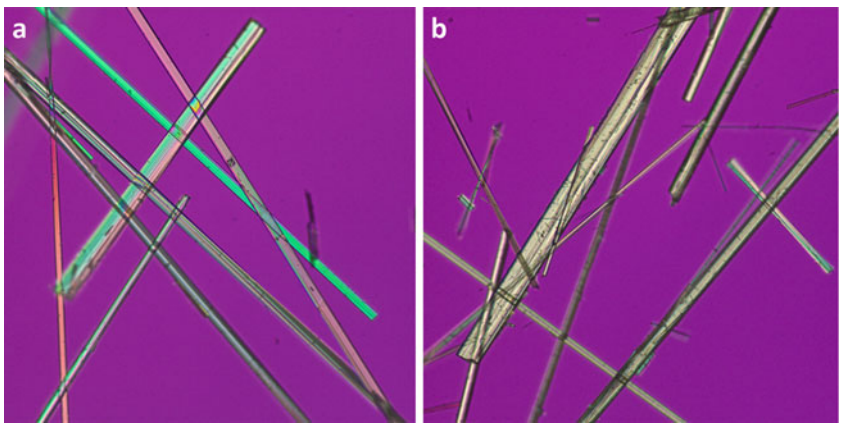

Fig. 3 Optical micrographs of TFA form I (**a**) and form II (**b**).

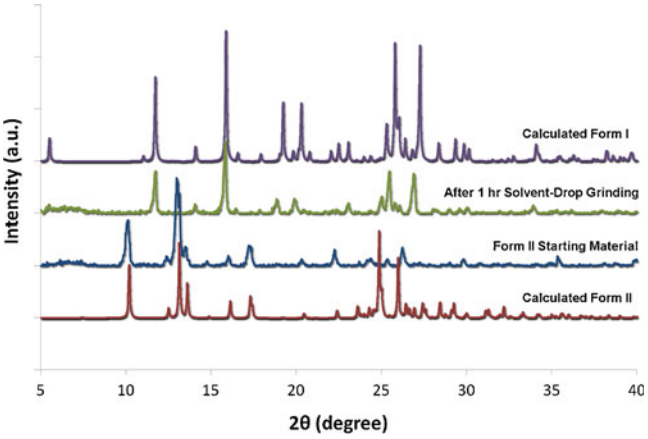

Fig. 5 X-ray powder patterns of TFA form II subjected to ethanol-assisted grinding.

pure form II converted to form I in a few hours at 25°C. DSC thermogram (Fig. 6) of form I shows melting of the crystal at the onset temperature of 212.5°C; the enthalpy of melting was 157.1 J/g. Form II shows two endothermic peaks. The first one with an enthalpy of 4.3 J/g and the onset temperature of 141.8°C appears to be a solid-solid phase transition to form I (inset of Fig. 6) and the second one at the onset temperature of 212.7°C is the melting of the transformed form I. These experiments indicate in cohort that form I of TFA is the thermodynamically stable polymorph.

Effect of Supersaturation on Crystal Growth of Tolfenamic Acid

Crystallization of TFA by crash cooling was conducted in ethanol. TFA concentration profiles were obtained at supersaturation ratios of S = 1.55, 1.70, and 1.95, respectively (Fig. 7). The solute concentration, detected by UV absorption, decreased with time, indicative of nucleation and growth of crystals. The process was monitored until the concentration reached progressively stable values. The final solute concentration values are in agreement with solubility of form I measured at 37°C. The figure also marks the apparent solubility of form II.

Crystallized solid samples were collected and analyzed to determine the polymorphic composition. PXRD analysis verified the solid-phase identity of these samples (Fig. 8), obtained at supersaturation ratio of S = 1.55 and isolated immediately after nucleation. The peak at 10.2° indicates that form II was present in the sample. In later collected samples, the peaks at 5.5° and 11.7° appeared, suggesting that any crystal of form II had transformed to polymorph I. ATR-FTIR spectra of pure forms I and II were obtained (Fig. 9a), as well as of known mixtures for quantifying the ratio between the two forms. The polymorph II spectrum exhibits a unique vibrational band at 1,521 cm^{-1} that clearly distinguishes it from form I. The peak at 1,327 cm^{-1} was chosen as the reference due to its insensitivity to the phase composition. The standard curve (Fig. 9b, R^2 of 0.996) was generated by plotting the ratio of the band intensities against the weight percentage of form II in the known solid mixture samples. Accordingly, the solid composition of collected solid samples at various time points was determined by FTIR analysis (Fig. 7, superimposed with the solute concentration profiles). At a lower supersaturation (S = 1.55 or 1.70), the metastable form II was initially obtained, followed by its transformation to the most stable form I, likely via a dissolution-recrystallization

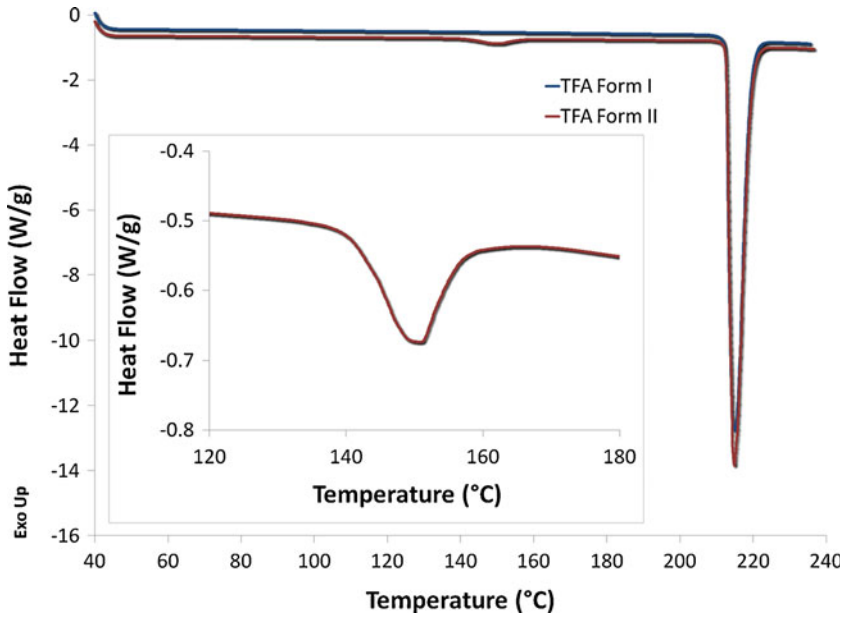

Fig. 6 DSC thermograms of pure TFA forms I and II. The inset shows the small endotherm due to phase transition of form II.

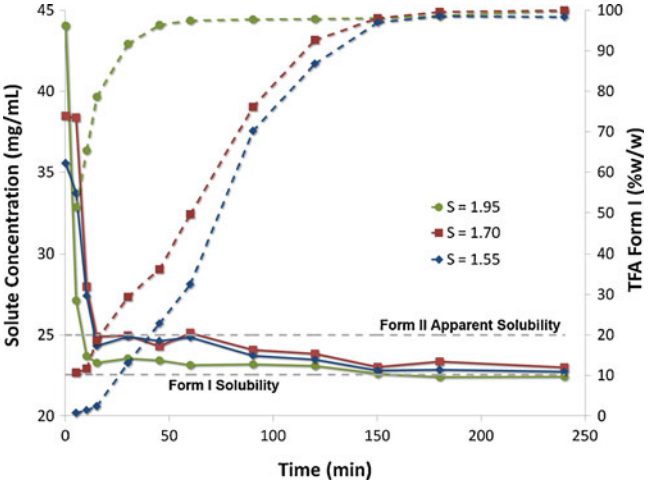

Fig. 7 Time dependence of concentration measured at 37°C during rapid cooling of TFA from ethanol at different initial supersaturations (S), 1.55, 1.70, and 1.95. The weight percentages of form I in the collected crystal samples are plotted correspondingly as dash lines. Solubility values of the two forms are marked as well.

mechanism (i.e., solvent-mediated phase transformation) (57–59). When S = 1.55, the solid-phase composition showed no onset presence of form I and the solute concentration kept at the solubility line of form II. Over the course of the transformation, a decrease in the amount of form II was associated with a concurrent increase in the quantity of form I while the concentration shifted to the solubility of form I. As the supersaturation increased, a mixture of both polymorphs was produced and, particularly when S = 1.95, form I became dominant and the solute concentration dropped to its solubility line quickly at the beginning of the experiment.

The results indicate a greater tendency to crystallize form I by increasing the initial solute concentration. When S = 1.55 or 1.70, the solvent-mediated phase transition from form II to form I may take dozens of minutes. Instead, the appearance of form I took a few minutes when S = 1.95,

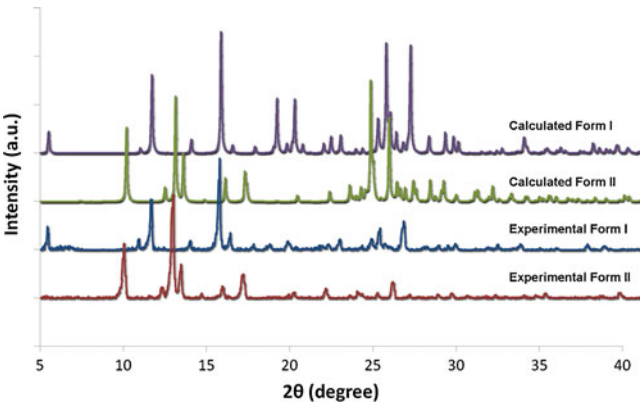

Fig. 8 X-ray powder patterns of TFA forms I and II obtained at S = 1.55. X-ray powder pattern of calculated forms I and II are also shown for comparison.

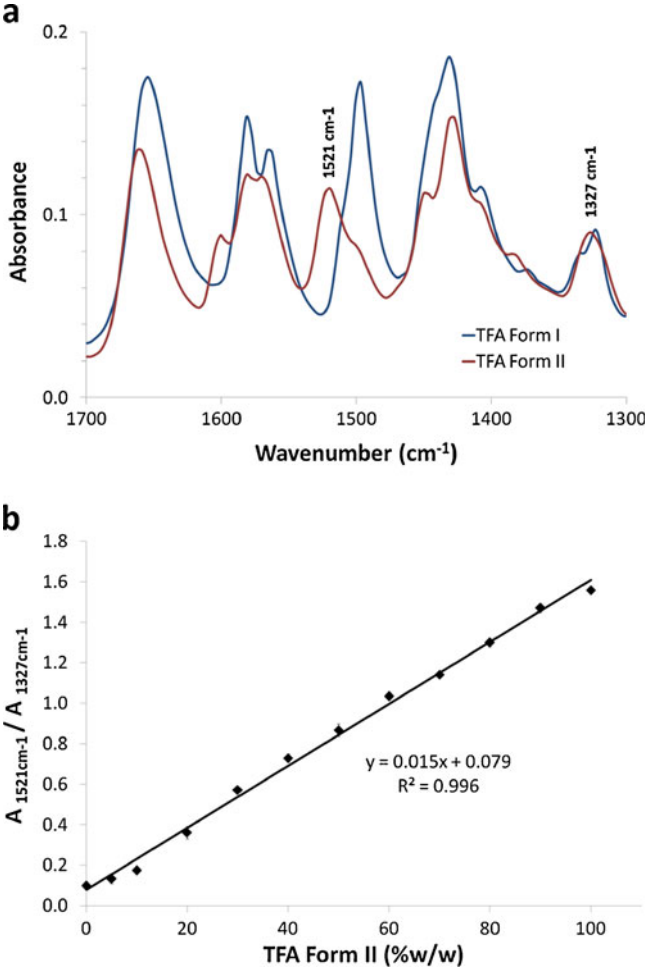

Fig. 9 Infrared spectra of TFA polymorphs (**a**) and standard curve of the relative concentration of form II in a mixture of TFA polymorphs (**b**). Measurement was done in triplicate to determine the standard curve.

indicating a result of not phase transformation from form II but a consequence of direct nucleation. Thus, although the final outcome of the crystallization experiments was the same (production of form I), two distinct mechanisms of crystal growth are plausible—depending on the supersaturation—and nucleation of the most stable form at high supersaturation apparently disobeys Ostwald's Rule of Stages (23).

To further elucidate the governing mechanism, seed crystals of both polymorphs were respectively introduced into solutions at the onset of cooling (Fig. 10). Addition of form I seeds resulted in an abrupt decrease of solution concentration, consistent with crystal growth of the seeds, until the solute concentration eventually reached the solubility of TFA form I (Fig. 10a). This was in agreement with the solid-phase composition determined by FTIR analysis (superimposed in Fig. 10a), where for all supersaturations the solid-phase was entirely constituted by form I. Following seeding with form II crystals (Fig. 10b), the metastable polymorph initially predominated and then it slowly converted into form I. During the polymorph

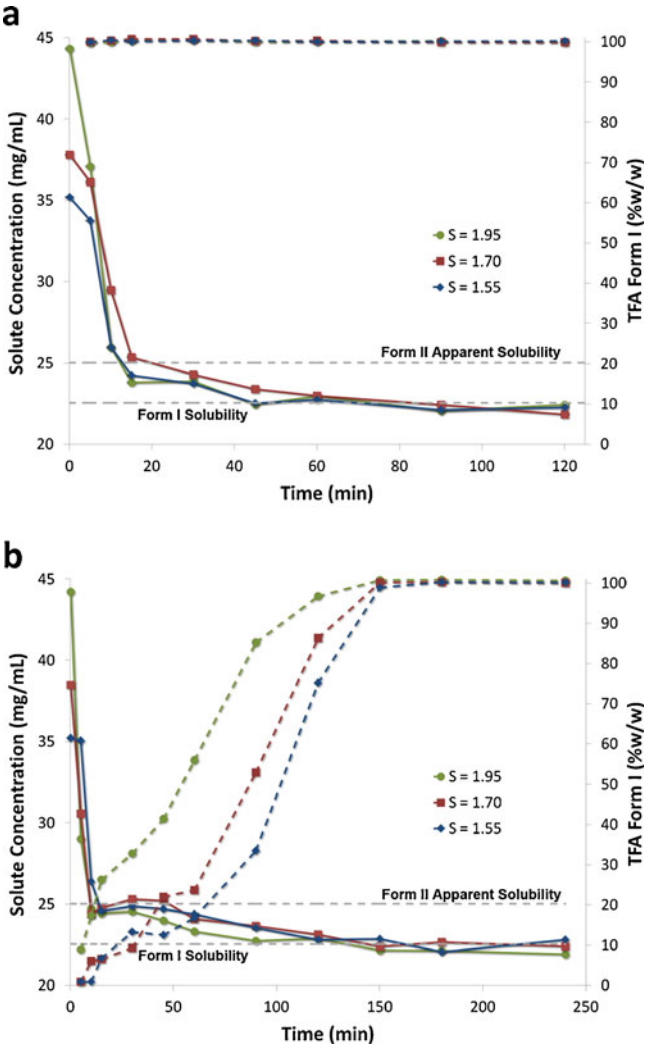

Fig. 10 Time dependence of concentration measured at 37°C during rapid cooling of TFA from seeded ethanolic solutions at different initial supersaturations (S), 1.55, 1.70, and 1.95 with seeds of form I (**a**) and seeds of form II (**b**). The weight percentages of form I in the collected crystal samples are plotted correspondingly as dash lines.

transformation, the solute concentration stayed at the apparent solubility of form II until the metastable crystals had completely dissolved and the concentration approached the solubility of form I. Consequently, the relative percentage of the solid form I increased during the transformation. No significant difference was found between the phase turnover when S = 1.55 or 1.70. When S = 1.95, a small amount of form I, about 9% relative to form II, also crystallized upon seeding with form II, possibly due to nucleation of form I despite the seeding. Overall, seeding crystals are able to essentially inhibit the nucleation step, particularly at low supersaturation. The experiments also rule out the possibility of competitive growth of the two polymorphs that may be affected by the solute concentration. If the two forms possess different concentration-dependent growth rates, seeding or no seeding should not affect the crystallization outcome. This is not what we observed and the results further confirm that, in the unseeded crystallization experiments, the nucleation mechanism is influenced by the supersaturation of solution.

Solution Chemistry

To understand the solution chemistry of the system, UV spectroscopy was performed to identify the likeliness and extent of aggregation of TFA solute molecules in ethanol as a function of concentration (below the solubility). The rationale lies in the fact that, prior to the crash cooling of crystallization, the TFA ethanol solutions were undersaturated but of different concentrations. The variation in concentration may affect how solute molecules behave in solution and consequently result in nucleation of the distinct species. By measuring UV absorbance at different concentrations, the molar absorptivity was calculated and plotted as a function of concentration (Fig. 11). Hypochromic deviation from the Beer-Lambert law is evident, suggesting self-association of solute molecules (43,60). The total absorbance may be regarded as a sum of individual species in the solution:

$$\varepsilon C_T = \varepsilon_m C_m + \varepsilon_n n K_{1,n} (C_m)^n \quad (1)$$

where ε is the apparent molar absorptivity determined from the experimental absorbance; ε_m and ε_n are the molar absorption coefficients of monomers and n-mer aggregates of solute molecules, respectively. In addition, n is the size of n-mer aggregates (i.e., 2 for dimer) and $K_{1,n}$ is the self-association equilibrium constant of the aggregation; C_T is the overall solute concentration and C_m the monomer concentration. The best fit of the experimental data based on Eq. 1 could then be obtained with a correlation

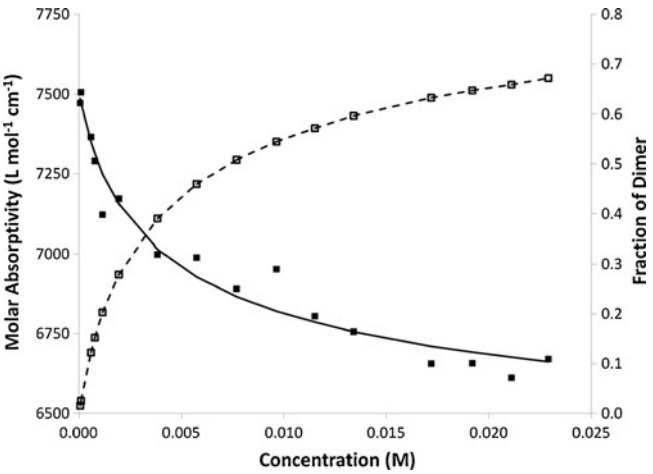

Fig. 11 Concentration dependence of the apparent molar absorptivity of TFA at $\lambda_{max} = 346$ nm. The solid line is a fit of the data according to Eq. 1; the dimer fraction is also shown as dash line *versus* the total TFA concentration.

coefficient of 0.98 (solid line in Fig. 11). The calculated value (± standard deviation) of $K_{1,n}$ is found to be 138.49 ± 34.25 M^{-1} and the corresponding n equals 2. Consequently, the dimer formation was derived (dash line in Fig. 11), indicating the trend of dimer association as the solute concentration increases. Thus, it is reasonable to speculate that when a solution of low concentration of TFA molecules is rapidly cooled (to become supersaturated), the dominant growth units are (solvated) monomers and, at high concentration, the units are mostly dimers. Although the dimer fraction was obtained at room temperature (Fig. 11) whereas the solutions in the crystallization experiments were cooled from 60°C, no significant variation in the association mode and the relative composition of various species is expected at modestly higher temperature (61). Note that the derived model assumes that dimers are the only species in equilibrium with monomer over the concentration range employed. Higher-order association species may be mathematically plausible (based on the data fitting), but to form them in solution seems unlikely or negligible. As pointed out by our computational analysis, intermolecular hydrogen-bonding of the dimers is much significant and hydrogen-bonded dimers should be dominant over other types of solute aggregates—if there are any—bonded by van der Waals force or even π-π stacking interactions. Still, further experimental evidence is needed and has been actively sought in our laboratory to support the concentration-dependent dimer formation.

Intermolecular Interactions

Both crystal structures of the TFA polymorphs consist of cyclic, hydrogen-bonded dimers (Fig. 2). The hydrogen-bonding energy of the form I dimer calculated by B3LYP is −37.65 kJ/mol per hydrogen bond (or −75.31 kJ/mol for two hydrogen bonds in a dimer) while that of the form II dimer is −34.60 kJ/mol. The energy values calculated by MP2 are −33.72 kJ/mol and −31.08 kJ/mol of the form I and form II dimer, respectively. Both methods indicate that the dimer of form I is stronger, by about 3 kJ/mol, than that of form II. As monomer, the form II conformer is more stable by 3–4 kJ/mol, calculated by DFT and MP2, respectively. In addition, the lattice energies of forms I and II are computed to be −137.50 and −135.72 kJ/mol, respectively, supporting the fact that form I is more stable than form II. The calculated lattice energy of form I is very close to a reported experimental value of the sublimation enthalpy of form I, 128.4 kJ/mol at 298 K (62), which yields a derived lattice energy value of −133.4 kJ/mol (see reference 49 for the derivation). Note that lattice energy is the energy difference between the energy of a crystal system and the lowest energy of a fully optimized single molecule in the gas phase. As such, the computed lattice energy values are evaluated based on the same molecular conformation. If the solute molecule already adjusts its conformation prior to nucleation and has the same conformation as that in the crystal, the energy change—more suitably, this may be called crystallization energy (63)—can be recalculated as the difference between energy of a crystal and its single molecule of the same conformation, yielding values of −249.17 and −241.38 kJ/mol for forms I and II, respectively. As no conformational change is considered, crystallization energy may better characterize the intermolecular interaction involved in the self-assembly process of crystallization in solution. Thus, if the dimers are considered as the growth units, it is argued that the hydrogen-bonding strength differentiates the formation of the two polymorphs from solution, as crystallization energy difference is on par with that of hydrogen-bonding between the two dimer motifs (about 6 kJ/mol if considering two hydrogen bonds in a dimer). The solvation energy is nonetheless overlooked in this discussion, but studies are underway to evaluate the solvent effect.

Nucleation Mechanism

Given the results of the crystallization experiments, solute species in solution, and intermolecular interaction calculations, the proposed mechanism implies that, when a solution of low concentration gets cooled and becomes supersaturated, the dominant solute monomers start to form nuclei. As the concentration increases, more self-association is warranted because of the thermodynamic driving force (i.e., chemical potential), and more hydrogen-bonded dimers form and dominate in solution. For the same thermodynamic reason, the solute molecules need to form dimers as strongly as possible and in the case of TFA, the molecules have to adjust their monomer conformations in order to form stronger hydrogen bonds (*ca.* 6 kJ/mol increase). The energy penalty due to the conformational change (*ca.* 3–4 kJ/mol) can be recovered from gaining a stronger hydrogen-bonding. When the condition of nucleation is met (i.e., an undersaturated solution is cooled), molecular clusters (i.e., dimers) start to form nuclei and initiate crystal growth. It is thus concluded that, when a solution of low TFA concentration is crash cooled, because the dominant solute species are (solvated) monomers, precursors of form II are produced leading to the growth of the yellow crystals. Conversely, when a solution of high TFA concentration reaches the nucleation condition, the strongly interacted hydrogen-bonded dimers act as building blocks for the growth of the colorless form I crystals. The key concept underpinning the argument is that, in order to form hydrogen-bonded dimers, solute molecules need to change their conformation from that in the monomer state. Thus, the self-association state of the solute species in solution determines the molecular conformation resembled in the final

crystal structure. As a concentration increase warrants further self-assembly of solute molecules, the effect of solute concentration on promoting hydrogen-bonded dimer formation and on polymorph selection is manifested by the conformational change of the solute. In other words, when the (solvated) monomers of TFA molecules start to be convened into dimers, the molecular conformation needs to change in order to facilitate the intermolecular hydrogen-bonding. More importantly, the argument implies the utmost role of solute species—monomers *vs.* dimers in our case—in governing the polymorphic formation from solution.

It is worth noting that the crash cooling condition in the crystallization experiments is not meant to freeze or maintain the relative ratios among various solute species during cooling. In fact, the relative ratios are controlled by molecular interactions and our cooling rate should not affect the association and conformational change processes, which should occur rapidly, based on the calculated values of the association constant and the energy barrier between the two conformers. The fast cooling rate is merely to prevent or minimize the solvent-mediated phase transition and timely probe the nucleation process.

CONCLUSIONS

Crystallization of a particular TFA polymorph in ethanol is affected by the starting concentration of the solute molecule. At low supersaturation, the metastable form was obtained while at high supersaturation, the most stable one was produced. As the concentration increases, hydrogen-bonded dimers become predominant in solution and overtake monomers as the nucleation unit. Thus, the self-assembly of solute molecules plays a pivotal role in nucleation of a different polymorphic structure and for this reason, the conformational energies and intermolecular interactions are the underlying factors determining pre-nucleation and nucleation processes. Moreover, the concentration effect highlights the limitation of CNT, which states that the supersaturation directly regulates the growth rate of a crystal system but not the rate difference among various polymorphs. Although further investigation is needed to better support the intricacy between molecular conformation in solution and packing in the solid state, the study offers a critical proof that pre-nucleation association of solute molecules, governed by molecular interactions and growth conditions, must be considered as an important stage of nucleation.

ACKNOWLEDGMENTS & DISCLOSURES

The authors recognize Dr. Roger Zanon from Upsher-Smith Laboratories for his suggestion of the seeding experiment and thank Profs. B. D. Anderson, Z. J. Hilt, and S. Van Lanen for their advices and instrument support. The study was supported by NSF (DMR-0449633 and DMR-1006364).

REFERENCES

1. Byrn SR, Pfeiffer RR, Stowell JG. Solid state chemistry of drugs. West Lafayette: SSCI, Inc.; 1999.
2. Hilfiker R. Polymorphism: in the pharmaceutical industry. Weinheim: Wiley-VCH; 2006.
3. Cote A, Zhou G, Stanik M. A novel crystallization methodology to ensure isolation of the most stable crystal form. Org Process Res Dev. 2009;13:1276–83.
4. Kee NCS, Tan RBH, Braatz RD. Selective crystallization of the metastable α-form of L-glutamic acid using concentration feedback control. Cryst Growth Des. 2009;9:3044–51.
5. Brittain HG. Polymorphism and solvatomorphism 2009. J Pharm Sci. 2011;100:1260–79.
6. Lahav M, Leiserowitz L. The effect of solvent on crystal growth and morphology. Chem Eng Sci. 2001;56:2245–53.
7. Long S, Parkin S, Siegler MA, Cammers A, Li T. Polymorphism and phase behaviors of 2-(phenylamino)nicotinic acid. Cryst Growth Des. 2008;8:4006–13.
8. Musumeci D, Hunter CA, McCabe JF. Solvent effects on acridine polymorphism. Cryst Growth Des. 2010;10:1661–4.
9. Jiang S, ter Horst JH, Jansens PJ. Concomitant polymorphism of o-aminobenzoic acid in antisolvent crystallization. Cryst Growth Des. 2008;8:37–43.
10. Kitamura M, Hironaka S. Effect of temperature on antisolvent crystallization and transformation behaviors of thiazole-derivative polymorphs. Cryst Growth Des. 2006;6:1214–8.
11. Lee EH, Byrn SR, Carvajal MT. Additive-induced metastable single crystal of mefenamic acid. Pharm Res. 2006;23:2375–80.
12. Lee EH, Boerrigter SXM, Rumondor ACF, Chamarthy SP, Byrn SR. Formation and solid-state characterization of a salt-induced metastable polymorph of flufenamic acid. Cryst Growth Des. 2008;8:91–7.
13. Kitamura M. Strategy for control of crystallization of polymorphs. CrystEngComm. 2009;11:949–64.
14. Etter MC. Hydrogen bonds as design elements in organic chemistry. J Phys Chem. 1991;95:4601–10.
15. Weissbuch I, Lahav M, Leiserowitz L. Toward stereochemical control, monitoring, and understanding of crystal nucleation. Cryst Growth Des. 2003;3:125–50.
16. Bernstein J, Etter MC, Leiserowitz L. In: Dunitz JD, Bürgi H-B, editors. Structure correlations. Weinheim: VCH; 1994. p. 431–507.
17. Chen J, Sarma B, Evans JMB, Myerson AS. Pharmaceutical crystallization. Cryst Growth Des. 2011;11:887–95.
18. Becker R, Döring W. Kinetische behandlung der keimbildung in übersättingten dämpfen. Ann Phys. 1935;24:719.
19. Volmer M. Kinetik der phasenbildung. Dresden: Steinkopf; 1939.
20. Kashchiev D, van Rosmalen GM. Review: nucleation in solutions revisited. Cryst Res Technol. 2003;38:555–74.
21. Myerson AS, Lo PY. Cluster formation and diffusion in supersaturated binary and ternary amino-acid solutions. J Cryst Growth. 1991;110:26–33.
22. Davey RJ, Allen K, Blagden N, Cross WI, Lieberman HF, Quayle MJ, *et al.* Crystal engineering—nucleation, the key step. CrystEngComm. 2002;4:257–64.
23. Ostwald W. Studien über die Bildung und Umwandlung fester Körper. Z Phys Chem. 1897;22:289–330.

24. Haisa M, Kashino S, Kawai R, Maeda H. Monoclinic form of para-hydroxyacetanilide. Acta Crystallogr. 1976;B32:1283–5.
25. Vekilov PG. Dense liquid precursor for the nucleation of ordered solid phases from solution. Cryst Growth Des. 2004;4:671–85.
26. Vekilov PG. Nucleation. Cryst Growth Des. 2010;10:5007–19.
27. Gavezzotti A. Molecular aggregation of acetic acid in a carbon tetrachloride solution: a molecular dynamics study with a view to crystal nucleation. Chem Eur J. 1999;5:567–76.
28. Shore JD, Perchak D, Shnidman Y. Simulations of the nucleation of AgBr from solution. J Chem Phys. 2000;113:6276–84.
29. Galkin O, Pan W, Filobelo L, Hirsch RE, Nagel RL, Vekilov PG. Two-step mechanism of homogeneous nucleation of sickle cell hemoglobin polymers. Biophys J. 2007;93:902–13.
30. Erdemir D, Lee AY, Myerson AS. Nucleation of crystals from solution: classical and two-step models. Acc Chem Res. 2009;42:621–9.
31. Asherie N, Lomakin A, Benedek GB. Phase diagram of colloidal solutions. Phys Rev Lett. 1996;77:4832–5.
32. Sommerdijk NAJM, de With G. Biomimetic CaCO3 mineralization using designer molecules and interfaces. Chem Rev. 2008;108:4499–550.
33. Pouget EM, Bomans PHH, Goos JACM, Frederik PM, de With G, Sommerdijk NAJM. The initial stages of template-controlled CaCO3 formation revealed by cryo-TEM. Science. 2009;323:1455–8.
34. Galkin O, Vekilov PG. Direct determination of the nucleation rates of protein crystals. J Phys Chem B. 1999;103:10965–71.
35. Davey RJ, Blagden N, Righini S, Alison H, Quayle MJ, Fuller S. Crystal polymorphism as a probe for molecular self-assembly during nucleation from solutions: the case of 2,6-dihydroxybenzoic acid. Cryst Growth Des. 2001;1:59–65.
36. Parveen S, Davey RJ, Dent G, Pritchard RG. Linking solution chemistry to crystal nucleation: the case of tetrolic acid. Chem Commun. 2005;12:1531–3.
37. Erdemir D, Chattopadhyay S, Guo L, Ilavsky J, Amenitsch H, Segre CU, *et al.* Relationship between self-association of glycine molecules in supersaturated solutions and solid state outcome. Phys Rev Lett. 2007;99:115702–4.
38. Yu L, Kingman NG. Glycine crystallization during spray drying: the pH effect on salt and polymorphic forms. J Pharm Sci. 2002;91:2367–75.
39. Gidalevitz D, Feidenhans'l R, Matlis S, Smilgies DM, Christensen MJ, Leiserowitz L. Monitoring *in situ* growth and dissolution of molecular crystals: towards determination of the growth units. Angew Chem Int Ed Engl. 1997;36:955–9.
40. Huang J, Stringfellow TC, Yu L. Glycine exists mainly as monomers, not dimers, in supersaturated aqueous solutions: implications for understanding its crystallization and polymorphism. J Am Chem Soc. 2008;130:13973–80.
41. Andersen KV, Larsen S, Alhede B, Gelting N, Buchardt O. Characterization of 2 polymorphic forms of tolfenamic acid, N-(2-methyl-3-chlorophenyl)anthranilic acid—their crystal structures and relative stabilities. J Chem Soc Perkin Trans 2. 1989;10:1443–7.
42. Lopez-Mejias V, Kampf JW, Matzger AJ. Polymer-induced heteronucleation of tolfenamic acid: structural investigation of a pentamorph. J Am Chem Soc. 2009;131:4554–5.
43. Morcillo J, Gallego E, Peral F. A critical study of the application of ultraviolet spectroscopy to the self-association of adenine, adenosine and 5′-AMP in aqueous solution. J Mol Struct. 1987;157:353–69.
44. Peral F, Gallego E. Self-association of pyrimidine and some of its methyl derivatives in aqueous solution. J Mol Struct. 1995;372:101–12.
45. Kelly SM, Jess TJ, Price NC. How to study proteins by circular dichroism. Biochim Biophys Acta Proteins Proteom. 2005;1751:119–39.
46. Frisch MJ, Trucks GW, Schlegel HB, Scuseria GE, Robb MA, Cheeseman JR, *et al.* Gaussian 03, Revision C.02. Wallingford: Gaussian Inc.; 2004.
47. Mammino L, Kabanda MM. A computational study of the interactions of the phloroglucinol molecule with water. J Mol Struct Theochem. 2008;852:36–45.
48. Boys SF, Bernardi F. Calculation of small molecular interactions by differences of separate total energies—some procedures with reduced errors. Mol Phys. 1970;19:553–66.
49. Feng S, Li T. Predicting lattice energy of organic crystals by density functional theory with empirically corrected dispersion energy. J Chem Theory Comput. 2006;2:149–56.
50. Li T, Feng S. Empirically augmented density functional theory for predicting lattice energies of aspirin, acetaminophen polymorphs, and ibuprofen homochiral and racemic crystals. Pharm Res. 2006;23:2326–32.
51. Kohn W, Meir Y, Makarov DE. Van der Waals energies in density functional theory. Phys Rev Lett. 1998;80:4153–6.
52. Dobson JF, McLennan K, Rubio A, Wang J, Gould T, Le HM, *et al.* Prediction of dispersion forces: is there a problem? Aust J Chem. 2001;54:513–27.
53. Dion M, Rydberg H, Schröder E, Langreth DC, Lundqvist BI. Van der Waals density functional for general geometries. Phys Rev Lett. 2004;92:246401–4.
54. Hepburn J, Scoles G, Penco R. A simple but reliable method for the prediction of intermolecular potentials. Chem Phys Lett. 1975;36:451–6.
55. Wu Q, Yang WT. Empirical correction to density functional theory for van der Waals interactions. J Chem Phys. 2002;116:515–24.
56. Dovesi R, Saunders VR, Roetti C, Orlando R, Zicovich-Wilson CM, Pascale F, *et al.* Crystal06 User's Manual. Torino: Universita' di Torino; 2006.
57. Cardew PT, Davey RJ. The kinetics of solvent-mediated phase-transformations. Proc R Soc London. 1985;A398:415–28.
58. Gu CH, Young V, Grant DJW. Polymorph screening: influence of solvents on the rate of solvent-mediated polymorphic transformation. J Pharm Sci. 2001;90:1878–90.
59. Zhang GGZ, Gu CH, Zell MT, Burkhardt RT, Munson EJ, Grant DJW. Crystallization and transitions of sulfamerazine polymorphs. J Pharm Sci. 2002;91:1089–100.
60. Rao CNR. Ultra-violet and visible spectroscopy. London: Butterworths; 1961.
61. Hughes CE, Hamad S, Harris KDM, Catlow CRA, Griffiths PC. A multi-technique approach for probing the evolution of structural properties during crystallization of organic materials from solution. Faraday Discuss. 2007;136:71–89.
62. Surov AO, Szterner P, Zielenkiewicz W, Perlovich GL. Thermodynamic and structural study of tolfenamic acid polymorphs. J Pharm Biom Anal. 2009;50:831–40. The sublimation enthalpies of TFA forms I and II were experimentally determined as 128.4 and 135.1 kJ/mol at 298 K, respectively. Note that the experimental value of sublimation enthalpy of form I was directly determined, but that of form II was estimated based on solution calorimetry data. Their claim of phase transition from form I to II in solution contradicts our observation.
63. Li T, Ayers PW, Liu SB, Swadley MJ, Aubrey-Medendorp C. Crystallization Force—a density functional theory concept for revealing intermolecular interactions and molecular packing in organic crystals. Chem Eur J. 2009;15:361–71.